IMPROVED DROUGHT EARLY WARNING AND FORECASTING TO STRENGTHEN PREPAREDNESS AND ADAPTATION TO DROUGHTS IN AFRICA

DEWFORA

A 7th Framework Programme Collaborative Research Project

Guidelines for downscaling and refinement of continental hydrological models to regional scale

WP4-D4.9

December 2013

Coordinator:	Deltares, The Netherlands
Project website:	www.dewfora.net
FP7 Call	ENV-2010-1.3.3.1
Contract no.	265454

Page intentionally left blank

DOCUMENT INFORMATION

Title	Guidelines for downscaling and refinement of continental hydrological models to regional scale
Lead Author	UNESCO-IHE
Contributors	ECMWF
Distribution	<Please select on of three below> PP: Restricted to other programme participants (including the Commission Services) RE: Restricted to a group specified by the consortium (including the Commission Services) CO: Confidential, only for members of the consortium (including the Commission Services)
Reference	WP4-D4.9

DOCUMENT HISTORY

Date	Revision	Prepared by	Organisation	Approved by	Notes
11/11/2013	1	P. Trambauer	UNESCO-IHE		
25/11/2013	2	S. Maskey	UNESCO-IHE		
03/12/2013	3	P. Trambauer	UNESCO-IHE		
09/12/2013	4	S. Maskey	UNESCO-IHE		
10/12/2013	5	P.Trambauer	UNESCO-IHE		
12/12/2013	6	E. Dutra	ECMWF		
13/12/2013	7	P. Trambauer	UNESCO-IHE		

ACKNOWLEDGEMENT

The research leading to these results has received funding from the European Union's Seventh Framework Programme (FP7/2007-2013) under grant agreement N°265454

Page intentionally left blank

SUMMARY

This report discusses spatial scale in hydrological modelling based on a "high" resolution-hydrological model for the Limpopo river basin (5 km × 5 km) and the original "low"-resolution hydrological model for Africa (50 km × 50 km). The results of four distributed fluxes: actual evaporation, direct runoff, subsurface flow, and baseflow for both models are analyzed and compared to assess the resolution effect on the model results. The bias between the two model results and the variability of the biases are used to compare the model. Moreover, the variation of the fluxes on high resolution grid cells within each low resolution grid cell is analyzed using the coefficient of variation.
This study also examines the potential of downscaling low resolution hydrological model results to the high resolution grid by considering only the signatures of the landscape in the high resolution. This was explored by classifying the landscape in wetlands, hillslopes and plateaus based on the height above the nearest drainage (HAND) and topographic slope, and assessing the variability of the high resolution results within each low resolution grid for each landscape class.

Comparable results were obtained from the low resolution model and the upscaled high resolution model for the evaporation flux. This was different for the other fluxes analysed. The variability of the high resolution results is to a large extent lower when distinction is made in the landscape (wetland, hillslope and plateau) than when no distinction is made. Results showed that there is good potential of downscaling the low resolution hydrological model results to high resolution based only on the terrain characteristics.

Page intentionally left blank

TABLE OF CONTENTS

1. INTRODUCTION 1

2. MATERIALS AND METHODS 3

2.1 GLOBALLY AVAILABLE SPATIAL DATA AND RESOLUTIONS FOR HYDROLOGICAL MODELLING 3
2.1.1 Topography 3
2.1.2 Land cover 3
2.1.3 Soil and subsurface structure 3
2.1.4 Climatic time series data 4

2.2 THE LIMPOPO RIVER BASIN 5

2.3 CONTINENTAL AND REGIONAL SCALE HYDROLOGICAL MODELS OF THE LIMPOPO BASIN 6
2.3.1 Description of the model 6
2.3.2 Data used for model set up and forcing 7

2.4 METHOD FOR COMPARING DISTRIBUTED FLUXES RESULTING FROM MODELS OF DIFFERENT SPATIAL RESOLUTIONS 9
2.4.1 Bias between high resolution and low resolution model results 9
2.4.2 Variability of fluxes at high resolution cell within a low resolution grid cell 9

2.5 HYDROLOGICAL DOWNSCALING BASED ON LANDSCAPE 10

3. RESULTS 11

3.1 COMPARISON OF DISTRIBUTED FLUXES FROM THE TWO MODELS 11
3.1.1 Actual evaporation 11
3.1.2 Direct runoff 13
3.1.3 Subsurface flow 15
3.1.4 Baseflow 17

3.2 VARIABILITY OF THE HIGH RESOLUTION FLUXES WITHIN EACH LOW RESOLUTION GRID CELL 18

3.3 HYDROLOGICAL DOWNSCALING OF LOW RESOLUTION FLUXES 22

4. CONCLUDING REMARKS 25

5. REFERENCES 27

LIST OF FIGURES

Figure 1 Location of the Limpopo river basin 5
Figure 2 Example of two parameter maps for the different model resolutions..... 7
Figure 3 Grid representation of the low and high resolution models..... 9
Figure 4 River discharge in Chokwe station (#24) 11
Figure 5 Mean (left) and standard deviation (right) of the annual relative bias *RB* for Actual evaporation. 12
Figure 6 Mean of the monthly relative bias *RB* for Actual evaporation. 12
Figure 7 Standard deviation of the monthly relative bias *RB* for Actual evaporation. 13
Figure 8 Mean (left) and standard deviation (right) of the annual relative bias *RB* for direct runoff. 14
Figure 9 Mean of the monthly relative bias *RB* for direct runoff. 14
Figure 10 Standard deviation of the monthly relative bias *RB* for direct runoff. 15
Figure 11 Mean (left) and standard deviation (right) of the annual relative bias *RB* for subsurface flow. 15
Figure 12 Mean of the monthly relative bias *RB* for subsurface flow. 16
Figure 13 Standard deviation of the monthly relative bias *RB* for subsurface flow. 16
Figure 14 Mean (left) and standard deviation (right) of the annual relative bias *RB* for baseflow ... 17
Figure 15 Mean of the monthly relative bias *RB* for baseflow..... 17
Figure 16 Standard deviation of the monthly relative bias *RB* for baseflow..... 18
Figure 17 Chosen latitude and longitude bands for the Hovmoller diagrams. 18
Figure 18 Latitude-time plots (top) and Longitude-time plots (bottom) of the grid (0.5°) monthly coefficient of variation of actual evaporation results from the high resolution model. 19
Figure 19 Latitude-time plots (top) and Longitude-time plots (bottom) of the grid (0.5°) monthly coefficient of variation of direct runoff results from the high resolution model. 20
Figure 20 Latitude-time plots (top) and Longitude-time plots (bottom) of the grid (0.5°) monthly coefficient of variation of subsurface flow results from the high resolution model. 21
Figure 21 Latitude-time plots (top) and Longitude-time plots (bottom) of the grid (0.5°) monthly coefficient of variation of baseflow results from the high resolution model. 21
Figure 22 HAND (left) and Slope (right) for the Limpopo river basin at a 0.05° resolution 22
Figure 23 Land features defined based on hand and slope: HAND < 15m: wetland, HAND > 15m and S>5%: hillslope, and HAND > 15m and S < 5%: plateau. 22
Figure 24 Latitude-time plots of the grid (0.5°) monthly coefficient of variation of direct runoff results from the high resolution model for the different landscape defined. 23

LIST OF TABLES

Table 1 Statistics for model evaluation..... 11

1. INTRODUCTION

Upscaling and downscaling methods are necessary to transfer information from small-scale data to large-scale predictions and vice versa. There are two approaches or methods for upscaling and downscaling. The first one involves dynamic models of parts of the hydrological cycle where the scaling issue is how the model equations and model parameters will change with scale. The second approach consists of statistical descriptions where the focus is on how to best represent random variability in both space and time at diverse scales (Blöschl, 2006). Even thought there is an vast amount of literature on upscaling and downscaling methods in the various subdisciplines of hydrology (Blöschl, 2006), downscaling is often heard of merely in climatology. On the other hand, upscaling of land surface and soil parameters, porous media, and climatological variables are widely cited (Stewart et al., 1996;Shuttleworth et al., 1997;Farmer, 2002).

Downscaling is a broadly used term in the field of atmospheric sciences , which Hewitson and Crane (1996) define as: "a term adopted ... to describe a set of techniques that relate local- and regional-scale climate variables to the larger scale atmospheric forcing". In atmospheric sciences, the dynamical downscaling approach involves a higher resolution climate model embedded within a global circulation model (GCM). In the statistical approach, statistical methods are used to establish empirical relationships between GCM-resolution climate variables and local climate (Fowler et al., 2007). Analogous with the climate downscaling, it is of interest to relate local- and regional-scale hydrological variables to the larger scale hydrological ones.

Hydrological models are commonly categorised based on how they represent 1) the physics of the processes involved (conceptual, empirical or physically based), and 2) the spatial discretization or resolution (distributed or lumped). Other classification exists, but these two already make a statement related to the spatial scale of the model. Whereas lumped model do not represent spatial variability explicitly, distributed models account for spatial variability at the defined scale by subdividing the landscape into several categories. Wigmosta and Prasad (2006) indicate that each type of model has a different problem with respect to scaling. They state that empirical models should not be scaled beyond the original range of development, conceptual models may introduce more or fewer phenomena as scale is changed and physically-based models employing distributed parameters for describing system variability have to confront the problem of variability as the resolution changes, making them the most challenging to scale.

In physically based hydrological models it is generally easier to upscale by aggregating outputs obtained at finer resolution than to downscale from a coarse resolution due to the difficulty of recovering details that were not present at the original scale (Wigmosta and Prasad, 2006). In some cases scaling may require a different mathematical representation of a particular process, and therefore the original model cannot be simply scaled but must be reformulated to include previously neglected processes. The model is said to be scalable when process equations, and model assumptions remain nearly valid under upscaling or downscaling of its variables, but rather the parameters require reconsideration to include the influences of spatial or temporal variability encountered at the extrapolated scale (Wigmosta and Prasad, 2006).

In this study we focus on the downscaling of these physically based scalable models where process equations remain invariant but parameters maps are specific for two defined resolutions (one is 100 times larger than the other one). We present some discussion and considerations on the downscaling and refinement of continental hydrological models to regional scale, based on a "high" resolution- hydrological model for the Limpopo river basin (5 km × 5 km) and the original "low"-resolution hydrological model for Africa (50 km × 50 km).

2. MATERIALS AND METHODS

2.1 GLOBALLY AVAILABLE SPATIAL DATA AND RESOLUTIONS FOR HYDROLOGICAL MODELLING

Inputs to a hydrological model require information on topography, land cover, soil and subsurface structure, and meteorological data. This information comes from different sources and very often they are available on different resolutions and formats. This of course is not ideal and needs to be addressed by aggregating or disaggregating the information to reach a common resolution. Moreover, for gridded or mapped data, the highest resolution in which input data can be obtained is already an average or representation of a specific area.

2.1.1 Topography

Digital elevation models (DEMs) are available with varying resolutions. Global DEMs are those which cover the entire earth surface and have a resolution of 1 km or higher. These DEMs include the GTOPO30 (30 arc-second resolution, approx. 1 km) from the USGS (https://lta.cr.usgs.gov/GTOPO30), and a higher quality DEM from the Advanced Spaceborne Thermal Emission and Reflection Radiometer (ASTER) instrument of the Terra satellite (http://asterweb.jpl.nasa.gov/gdem.asp) which is available for 99% of the globe with a 30 meter resolution. Finer DEMs exist with resolutions up to 5 m, but are local to specific areas. For any grid resolution, sub-grid variability of course exists but this information is generally unavailable or lost through interpolation techniques (Wechsler, 2007).

2.1.2 Land cover

Four global land cover maps derived from remotely sensed data are freely available, all of which have a spatial resolution of 1 km. Three of them are developed in the United States: GLCC USGS (Loveland et al., 2000), UMD GLCM (Hansen et al., 2000), and Boston MODIS (Friedl et al., 2002). These data sets are in accordance with the IGBP classification system with 17 categories of cover types. The fourth one is the Global Land Cover 2000 (GLC2000) developed in Europe (Fritz et al., 2003) and has a 22 category classification scheme adopted from the Food and Agricultural Organization (Peng, 2008).

2.1.3 Soil and subsurface structure

The Harmonized World Soil Database (HWSD) is a 30 arc-second (approximately 1 km) raster database with over 15,000 different soil mapping units that combines existing regional and national updates of soil information worldwide with the information contained within the 1:5,000,000 scale FAO-UNESCO Soil Map of the World. Several other soil datasets are available (including soil types at 0.5° and 1°, and other several soil properties at 0.5°) at the US ORNL Distributed Active Archive Center (THREDDS Data Server Catalog Service).

Moreover, the FAO (http://www.fao.org/nr/land/soils/en/) digital soil map of the world (FAO, 2003) and related properties are available as a vector data set and are based on the FAO-UNESCO Soil Map of the World and digitized at 1:5.000.000 scale. The ISRIC - World Soil Information dataholdings (http://www.isric.org/) contain a wide selection of soil datasets including several soil properties at 1km resolution.
Regarding lithology, a new high resolution global lithological map (GLiM ,with an “average” scale of 1:3,750,000) allows observation of regional lithological distributions (Hartmann and Moosdorf, 2012). Hartmann and Moosdorf (2012) described other three older digital global lithological maps that are available: two of them are grid-based representations with a resolution of 2° (Bluth and Kump, 1991) and 1° (Amiotte Suchet et al., 2003), and the third one is a vector-map translated from the second edition of a geological world map at a scale of 1:25,000,000 using additional literature (Dürr et al., 2005).

2.1.4 Climatic time series data

Meteorological data is available from numerous sources at different spatial resolutions. Several satellite-based rainfall estimates (SRFE) are available globally with resolutions ranging around 0.1° - 0.25°. Reanalysis data sets incorporate observations and outputs from numerical weather prediction (NWP) models. The resolutions are generally lower, in the order of 1° (ERA-Interim has a horizontal resolution of approximately 0.7°). Other widely used products for precipitation include: 1) the GPCP v2.1 (product of the Global Precipitation Climatology Project, http://precip.gsfc.nasa.gov/) which is provided monthly globally at 2.5˚ × 2.5˚ resolution (or 1° for daily data) and combine precipitation information from several sources. 2) Global Precipitation Analysis Products of the Global Precipitation Climatology Centre (GPCC) which is gauge-based gridded monthly precipitation data sets for the global land surface at resolutions of 1°and 2.5° for all products; and 0.5° for non-real time products (http://gpcc.dwd.de/). The CRU TS 2.0 global dataset comprises monthly grids of observed climate for the period 1901-2000 at a resolution of 0.5°. The dataset includes five climatic variables: cloud cover, DTR, precipitation, temperature, vapor pressure (http://data.giss.nasa.gov/precip_cru/).

Based on the scale availability of spatial input data, we can point out that 1 km is the smallest grid scale on which we can set up a large scale hydrological model with available input global data. However, we should define the best resolution to use in each case by considering the basin size, purpose of the modelling, required results, and computation time.

2.2 THE LIMPOPO RIVER BASIN

The Limpopo river basin has a drainage area of approximately 415,000 km^2 and is shared by four riparian countries: South Africa (45%), Botswana (20%), Mozambique (20%) and Zimbabwe (15%) (see Figure 1). The climate in the basin ranges from tropical dry savannah and hot dry steppe to cool temperatures in the mountainous regions. Although a large part of the basin is located in a semi-arid area the upper part of the basin is located in the Kalahari Desert where it is particularly arid. The aridity condition, however, decreases further downstream. Rainfall in the basin is characterized by being seasonal and unreliable causing frequent droughts, but floods can also occur in the rainy season The average annual rainfall in the basin is 530 mm year^{-1}, ranging from 200 to 1,200 mm year^{-1} and occurring mainly in the summer months (October to April) (LBPTC, 2010). Two distinct seasons are identified in the basin: a summer and rainy season with about 95% of the annual rainfall, and a winter and dry season (DEWFORA, 2012b). For a detailed description of the Limpopo River basin the readers are referred to a previous report of this project: Deliverable 6.1, chapter 6 (DEWFORA, 2012a).

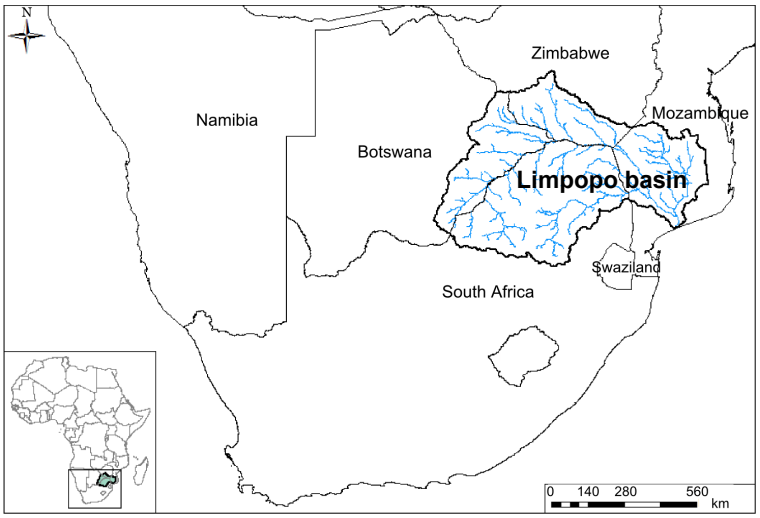

Figure 1 Location of the Limpopo river basin

This basin is particularly challenging for hydrological modeling – which is probably also true for many other arid/semi-arid basins – due to very low runoff coefficient (RC = *Q*/*P*) of the basin. For Chokwe station (station with largest drainage area with available data), for example, the runoff coefficient is just about 3.1% for the naturalized discharge and merely 0.4% for the observed discharge (without naturalization). Note that the naturalized discharge is estimated as observed discharge plus the estimated extraction. These runoff coefficients are strikingly low: out of 506 mm of annual rainfall only 18 mm (basin average) turned into runoff annually including abstraction.

2.3 CONTINENTAL AND REGIONAL SCALE HYDROLOGICAL MODELS OF THE LIMPOPO BASIN

2.3.1 Description of the model

A processed based distributed hydrological (water balance) model based on PCR-GLOBWB (van Beek and Bierkens, 2009) is used. The PCR-GLOBWB was one of the 16 different land surface and hydrological models reviewed (Trambauer et al., 2013 ;DEWFORA, 2011) in the DEWFORA project, and identified as one of the hydrological models that can potentially be used for hydrological drought studies in large river basins in Africa. PCR-GLOBWB is in many ways similar to other global hydrological models, but it has many improved features, such as improved schemes for sub-grid parameterization of surface runoff, interflow and baseflow, a kinematic wave based routing for the surface water flow, dynamic inundation of floodplains and a reservoir scheme (van Beek and Bierkens, 2009;van Beek, 2008).
On cell-by-cell basis and a daily time step, it computes the water storage in two vertically stacked soil layers (max. depth 0.3 and 1.2 m) and an underlying groundwater layer, as well as the water exchange between the layers and between the top layer and the atmosphere. It also calculates canopy interception and snow storage. Within a grid cell, the sub-grid variability is taken into account considering tall and short vegetation, open water and different soil types. The total specific runoff of a cell consists of the surface runoff (saturation excess), snowmelt runoff (after infiltration), interflow (from the second soil layer) and baseflow (from the lowest reservoir as groundwater). River discharge is calculated by accumulating and routing specific runoff along the drainage network and including dynamic storage effects and evaporative losses from lakes and wetlands. Other results of the hydrological model include: actual evaporation; soil moisture; root stress, water storage in the three layers, and other hydrological parameters.

The PCR-GLOBWB global hydrological model was first adapted to the continent Africa (DEWFORA, 2012b). The continental model (0.5˚ x 0.5˚) was trimmed for the Limpopo river basin without any change in resolution, resulting in the ***"low-resolution"*** Limpopo hydrological model. Moreover, a downscaled or ***"high-resolution"*** model was setup for the Limpopo river basin, where all the input parameters are derived at a resolution of 0.05˚ (approximately 5 km). Both models have a daily temporal resolution.

Both models were run for the period January 1979- December 2010 with the input parameter and meteorological data described. In the current versions of the model no calibration has been applied. The idea is that a process based distributed model should be applied with minimal calibration, particularly when they are applied in a large basin (Maskey and Trambauer, 2013).

2.3.2 Data used for model set up and forcing

INPUT PARAMETER MAPS

The Digital Elevation Model (DEM) is based on the Hydro1k Africa (USGS EROS, 2006). The majority of the parameters (maps) required for the models (e.g. soil layer depths, soil storage capacity, hydraulic conductivity etc.) were derived mainly from three maps and their derived properties: the Digital Soil Map of the World (FAO, 2003), the distribution of vegetation types from GLCC (USGS EROS, 2002;Hagemann, 2002), and the lithological map of the world (Dürr et al., 2005) (DEWFORA, 2012b). These parameters where upscaled to the two different resolutions. An example of two parameter maps (saturated conductivity on the second layer (ks2) and the depth of the first layer (z1)) are presented in Figure 2 for the two different models.

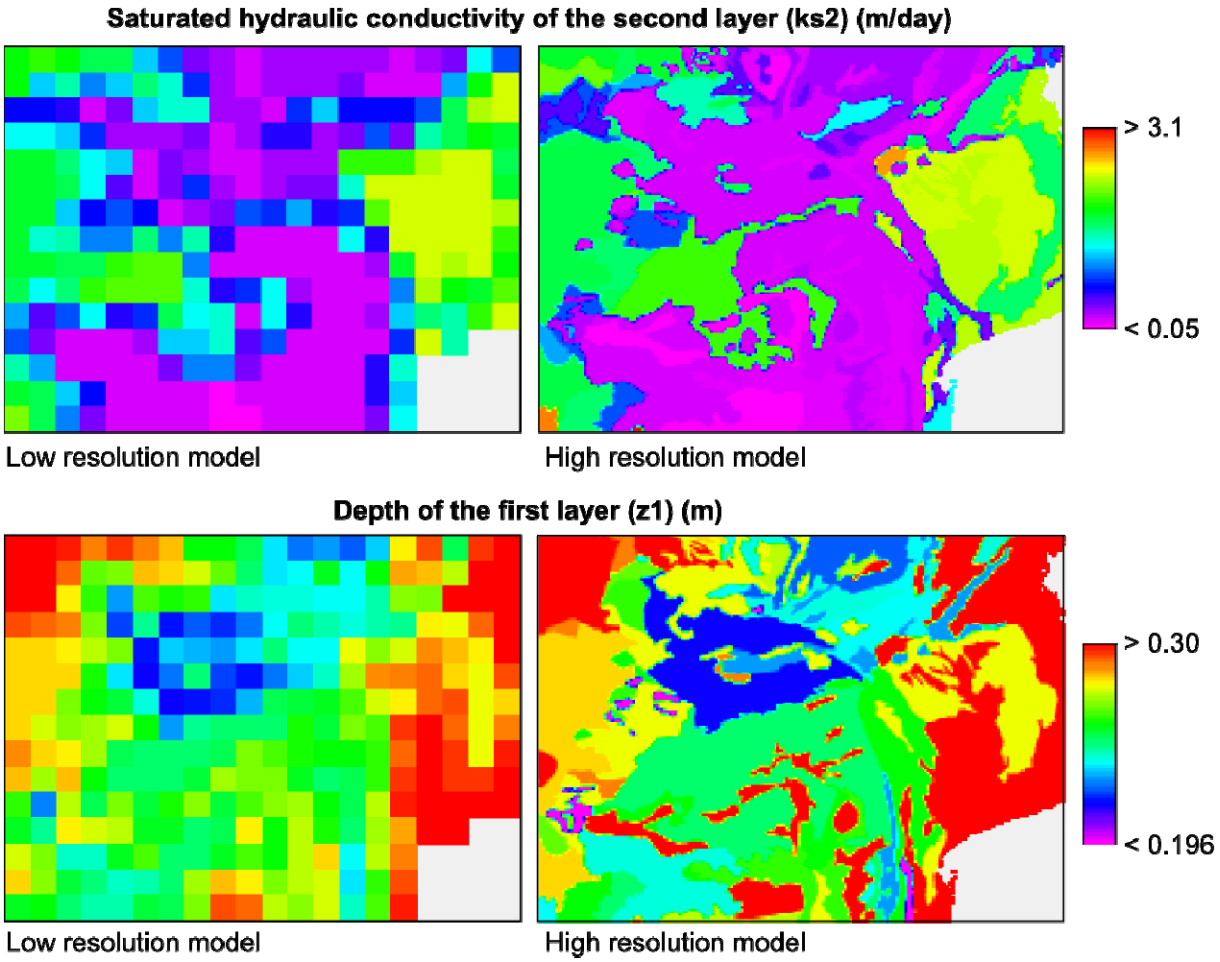

Figure 2 Example of two parameter maps for the different model resolutions

The irrigated area was obtained from the global map of irrigated areas in 5 arc-minutes resolution based on Siebert et al. (2007) and FAO (1997). We computed the monthly irrigation intensities per grid cell using the irrigated area map, the irrigation water requirement data per riparian country of the basin (DEWFORA, 2012a) and the irrigation cropping pattern zones (FAO, 1997).

METEOROLOGICAL DATA

All the meteorological forcing data (precipitation, daily minimum and maximum temperature at 2 meter) used are based on ERA-Interim (ERAI) reanalysis dataset from the European Centre for Medium-Range Weather Forecasts (ECMWF). This dataset covers the period from January 1979 to present date with a horizontal resolution of approximately 0.7 degrees and 62 vertical levels. A comprehensive description of the ERAI product is available in Dee et al. (2011). The ERA-Interim precipitation data used with the present model were corrected with GPCP v2.1 (product of the Global Precipitation Climatology Project) to reduce the bias with measured products (Balsamo et al., 2010). The GPCP v2.1 data are the monthly climatology provided globally at 2.5˚ × 2.5˚ resolution, covering the period from 1979 to September 2009. The data set combines the precipitation information available from several sources (satellite data, rain gauge data, etc.) into a merged product (Huffman et al., 2009;Szczypta et al., 2011). From September 2009 to December 2010, the mean monthly ERAI precipitation was corrected using a mean bias coefficient based on the climatology of the bias correction coefficients used for the period 1979-2009. While this only corrects for systematic biases, this was the only option available at the time, as a new version of GPCP (version 2.2) was not available. Temperature data is used for the computation of the reference potential evaporation needed to force the hydrological model. In this study the Hargreaves formula was used. This method requires less parameterization than Penman-Monteith, with the disadvantage that it is less sensitive to climatic input data, with a possibly reduction of dynamics and accuracy. However, it leads to a notably smaller sensitivity to error in climatic inputs (Hargreaves and Allen, 2003). Moreover, the choice of the method used for the computation of the reference potential evaporation seems to have minor effects on the results of the hydrological model for Southern Africa (Trambauer et al., 2013). For this study, the ERAI data were obtained for the period of 1979-2010 at a resolution of 0.5˚, after a bilinear interpolation from the original resolution of 0.7°, covering the entire African continent.

MEASURED RUNOFF

Runoff data were obtained from the Global Runoff Data Centre (GRDC; http://grdc.bafg.de/), the Water Affairs Republic of South Africa and ARA-Sul (Administração Regional de Águas, Mozambique). Most of the runoff data stations which were available for the relatively recent years and with relatively less missing data are in the South African part of the basin as almost no data could be found from stations in the other countries.

2.4 METHOD FOR COMPARING DISTRIBUTED FLUXES RESULTING FROM MODELS OF DIFFERENT SPATIAL RESOLUTIONS

From both hydrological models resolutions (L: low and H: high), we analyzed the results of four distributed fluxes: actual evaporation (mm month^{-1}), direct runoff (mm month^{-1}), subsurface flow (mm month^{-1}), and baseflow (mm month^{-1}). We compared the upscaled results of the high resolution model ($\overline{Q_H}$) with the results of the low resolution model (Q_L), and we analyzed the variability of the high resolution results within each low resolution grid cell.

2.4.1 Bias between high resolution and low resolution model results

For each monthly (or annual) variable *Q*, the low resolution (Q_L) and high resolution (Q_H) results were compared in the following way:

1. For each month (or year), the 100 high resolution pixels within each low resolution pixel (see Figure 3) were averaged ($\overline{Q_H} = \frac{\sum Q_H}{100}$).
2. The relative bias *RB* was defined to compare the two maps as: $RB = \frac{(\overline{Q_H} - Q_L)}{\overline{Q_H}}$. This results in a map of *RB* for each month (or year).
3. The mean and standard deviation of the *RB* time series were computed and are presented both yearly and monthly.

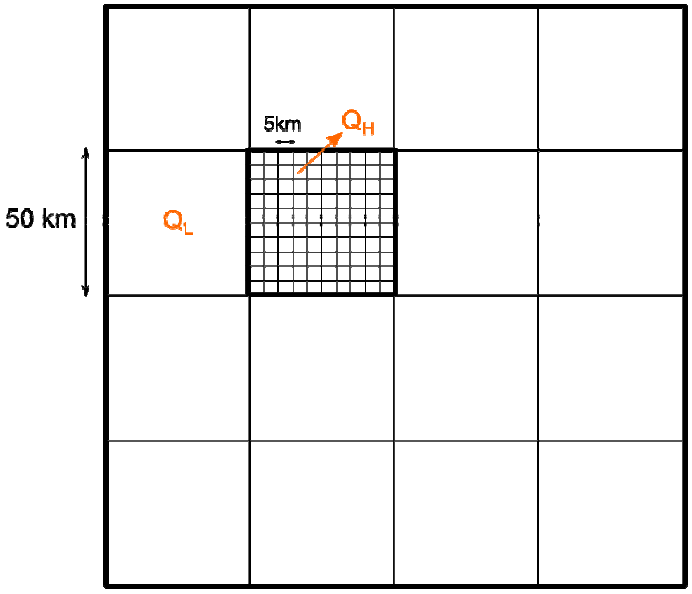

Figure 3 Grid representation of the low and high resolution models

2.4.2 Variability of fluxes at high resolution cell within a low resolution grid cell

The variability of the high resolution variables within each low resolution pixel was assessed using the coefficient of variation ($CV = \frac{\sigma}{\mu}$, defined as the ratio of the standard deviation σ to the mean μ). The resulting time series of *CV* maps are easily visualized in an animation. Here we present the maps of CV in time-latitude and time-longitude plots (Hovmoller diagram) for selected longitude and latitude bands.

2.5 HYDROLOGICAL DOWNSCALING BASED ON LANDSCAPE

This section investigates the possibility of downscaling the low resolution hydrological model (0.5° resolution grid) to the high resolution grid (0.05°) by taking into consideration only the signatures of the landscape in the high resolution. The idea is that the results from the low resolution continental scale hydrological model can be transferred to local scale by identifying spatial patterns based only on topographical features. The topography characteristics used here are the height above the nearest open water (HAND, Rennó et al., 2008) and slope (S). HAND has been identified as a powerful tool to be used for hydrological classification; it allows distinction between wetlands, hill slopes and plateaus (Savenije, 2010). We computed the maps of HAND and slope in the 0.05° resolution and based on this information we classified the landscape in these 3 land features.

We analyzed the variability of the high resolution model results within each low resolution grid cell but independently for the three land features defined. The point here is to observe if the variability of the high resolution results within each land feature is smaller than the case with no distinction of the land features.

3. RESULTS

The river discharge at Chokwe station (station with largest drainage area with available data) for both resolution models together with observations are presented in Figure 4. It can be observed that the results from both models are quite similar, but in general the higher resolution model approximates more to the observed discharge.

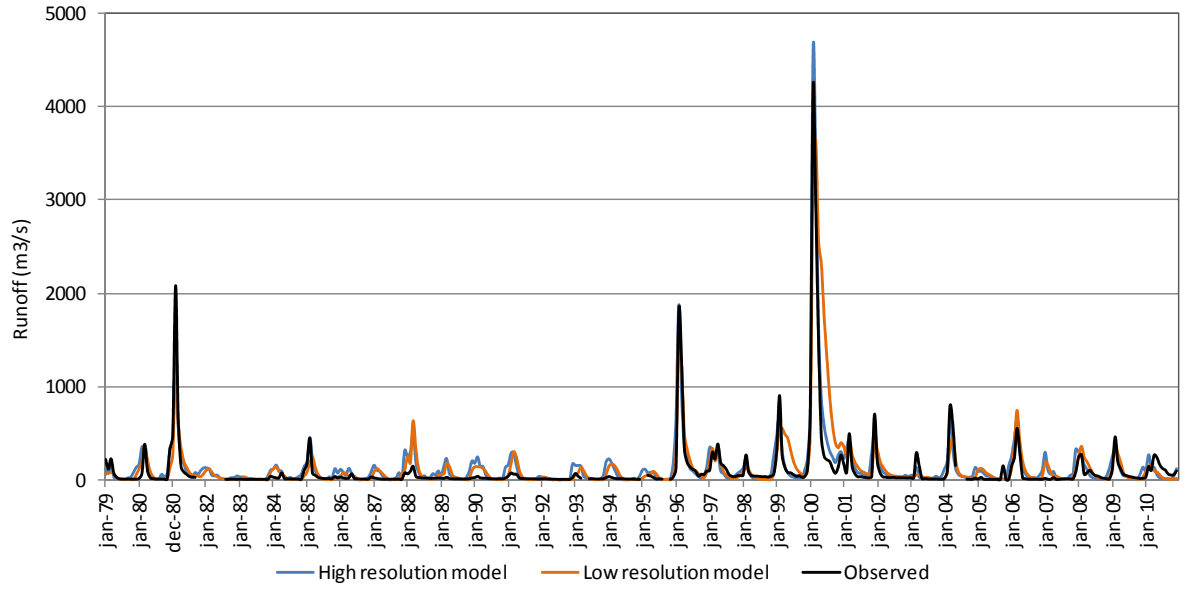

Figure 4 River discharge in Chokwe station (#24)

Table 1 presents three quantitative statistics for model evaluation: coefficient of determination (R^2), Nash-Shutcliffe efficiency (NSE), and ratio of the root mean square error to standard deviation of measured data (RSR). Moriasi et al. (2007) specified ranges for two of these statistics for a "satisfactory" model performance (NSE > 0.5, RSR ≤ 0.70). Based on these three statistics both models perform reasonably well, but the high resolution model performs better.

Table 1 Statistics for model evaluation

	High res. model	Low res. model
R^2	0.92	0.73
NSE	0.90	0.66
RSR	0.32	0.58

3.1 COMPARISON OF DISTRIBUTED FLUXES FROM THE TWO MODELS

3.1.1 Actual evaporation

We first computed the time series of relative bias (*RB*) from the actual evaporation results of the two resolutions models. The mean and standard deviation of the *RB* were then computed both yearly (Figure 5) and monthly (Figure 6 and Figure 7).

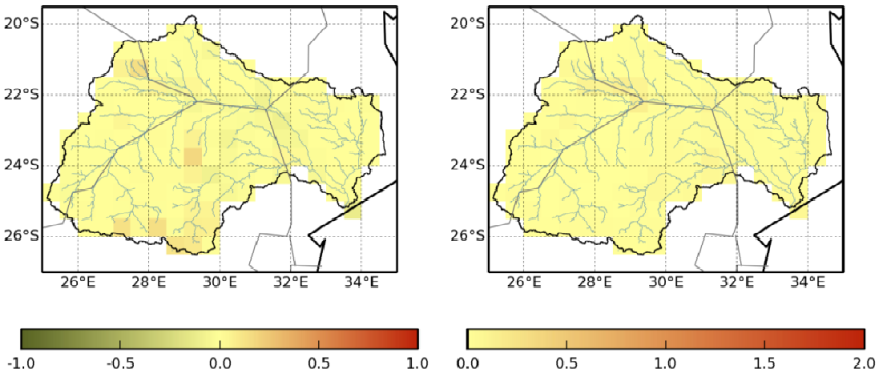

Figure 5 Mean (left) and standard deviation (right) of the annual relative bias *RB* for Actual evaporation.

Figure 5 shows that in an annual basis the bias between the actual evaporation results of the low resolution model and the average of the high resolution model over the low resolution grid is negligible, meaning that almost the same results in annual evaporation can be obtained with either of the model resolutions. From Figure 6 and Figure 7 it can be observed that the highest bias between the two products concerning evaporation occur during the dry season, mainly from May to September. These are also the months for which high standard deviations of the relative bias are observed.

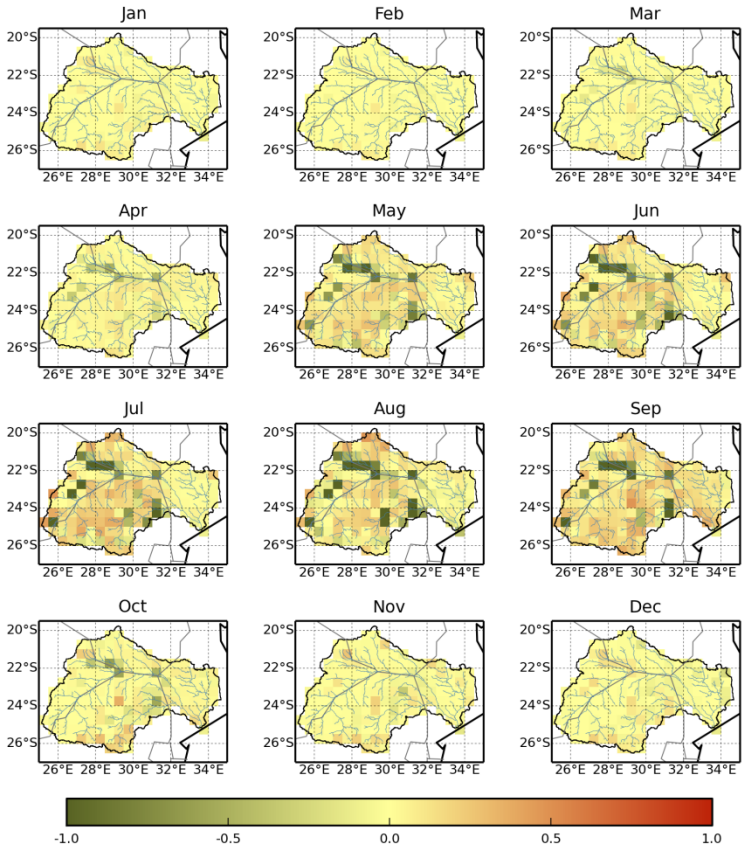

Figure 6 Mean of the monthly relative bias *RB* for Actual evaporation.

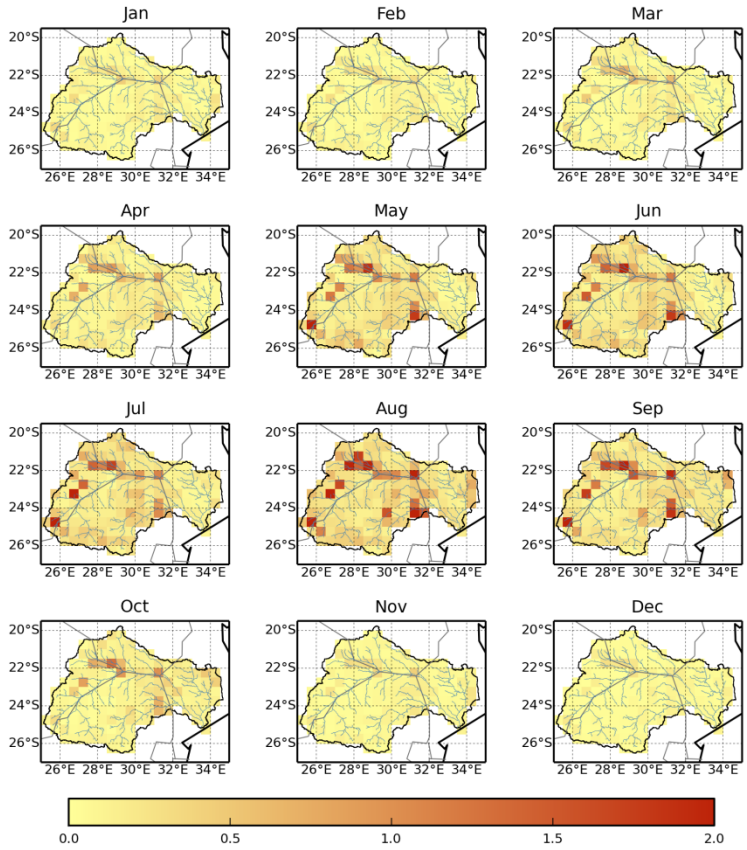

Figure 7 Standard deviation of the monthly relative bias *RB* for Actual evaporation.

3.1.2 Direct runoff

Likewise, we computed the mean and standard deviation from the time series of relative bias (*RB*) of the direct runoff results of the two resolutions models, both yearly (Figure 8) and monthly (Figure 9 and Figure 10). Figure 8 shows that in an annual basis the relative bias between the direct runoff results of the low resolution model and the average of the high resolution model over the low resolution grid is in general equal or almost equal to one. This means that in general the annual direct runoff from the low resolution model is zero or almost zero, which is quite expected for such a low resolution model. The standard deviation of the annual relative bias is in general close to zero, meaning that in large part of the basin the relative bias is similar year to year. Similar results are obtained on a monthly basis (see Figure 9 and Figure 10). There are few areas, however, where the direct runoff or the low resolution model is higher than the one of the high resolution model mostly during the rainy season. In these areas is where the standard deviation is higher, i.e. a higher variability between years/months is observed.

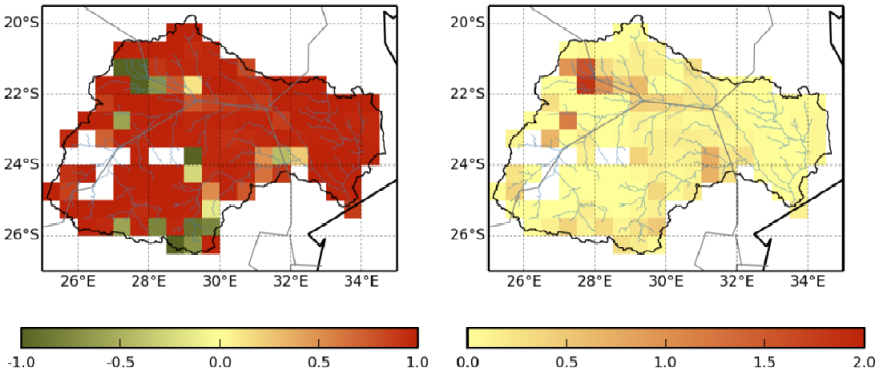

Figure 8 Mean (left) and standard deviation (right) of the annual relative bias *RB* for direct runoff.

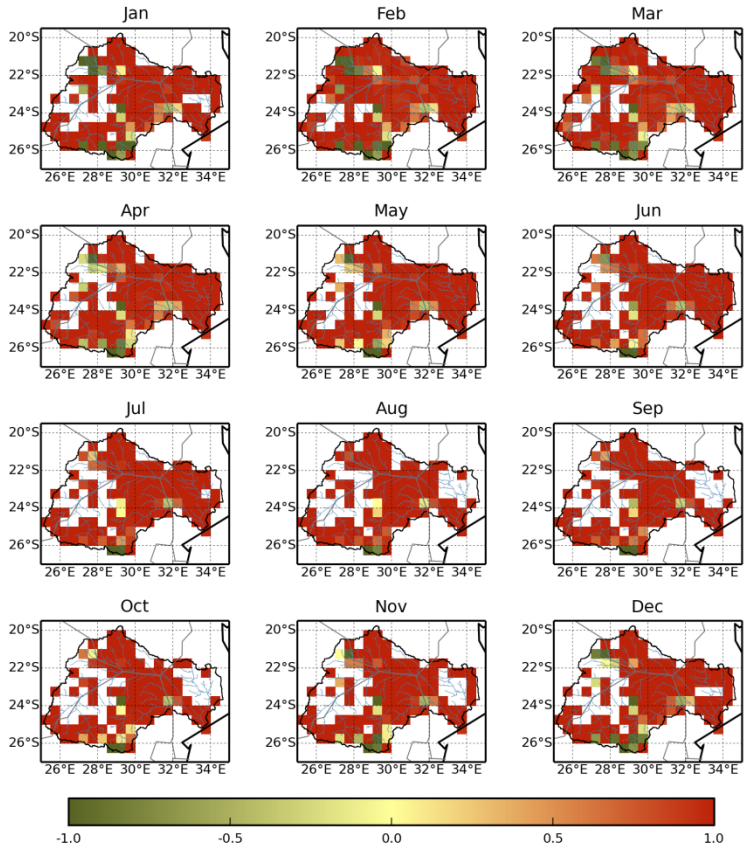

Figure 9 Mean of the monthly relative bias *RB* for direct runoff.

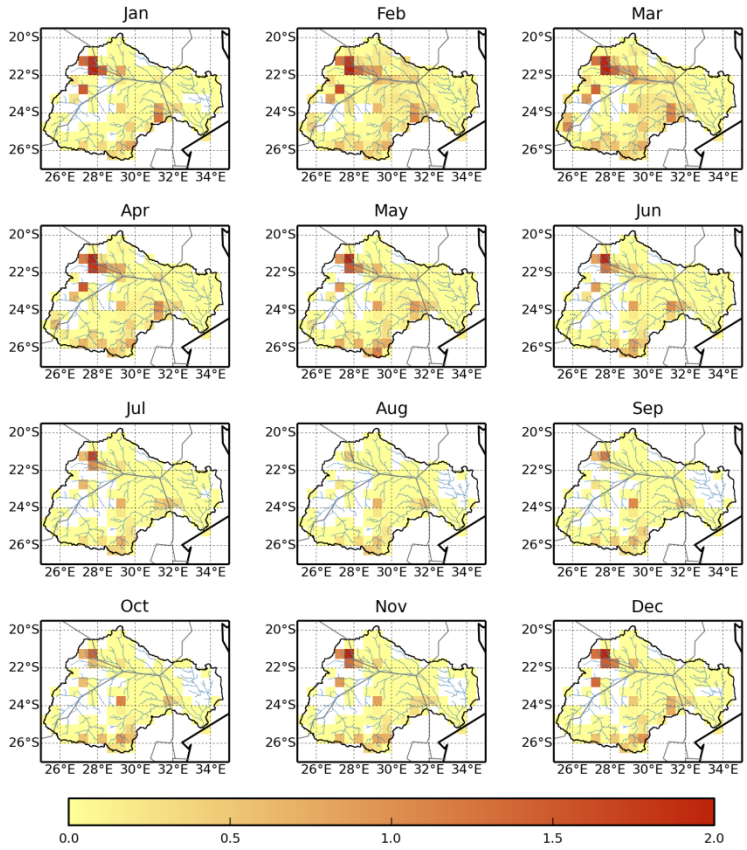

Figure 10 Standard deviation of the monthly relative bias *RB* for direct runoff.

3.1.3 Subsurface flow

The mean and standard deviation from the time series of relative bias (*RB*) of the subsurface flow results of the two resolutions models are presented in Figure 11 (yearly) and Figure 12 and Figure 13 (monthly). For the subsurface flow both annual and monthly the mean of the RB is generally between 0.5 and 1, meaning that the high resolution model in general results in higher values than the low resolution model. However, there are several grids where the opposite occurs (RB is lower than zero). For this flux, the standard deviation of the RB is higher than for the other two fluxes discussed.

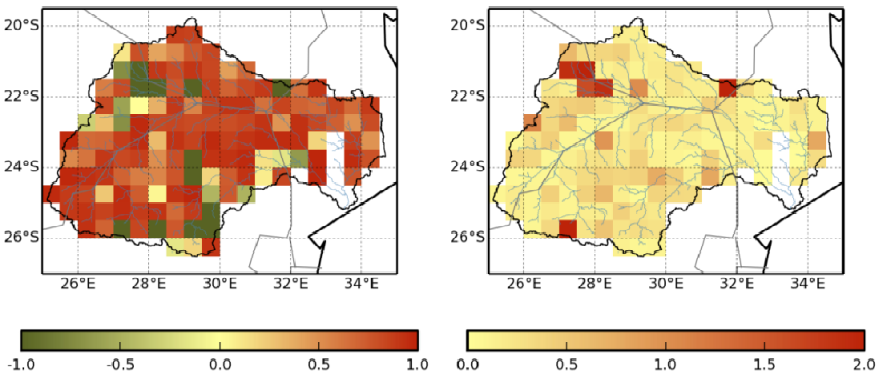

Figure 11 Mean (left) and standard deviation (right) of the annual relative bias *RB* for subsurface flow.

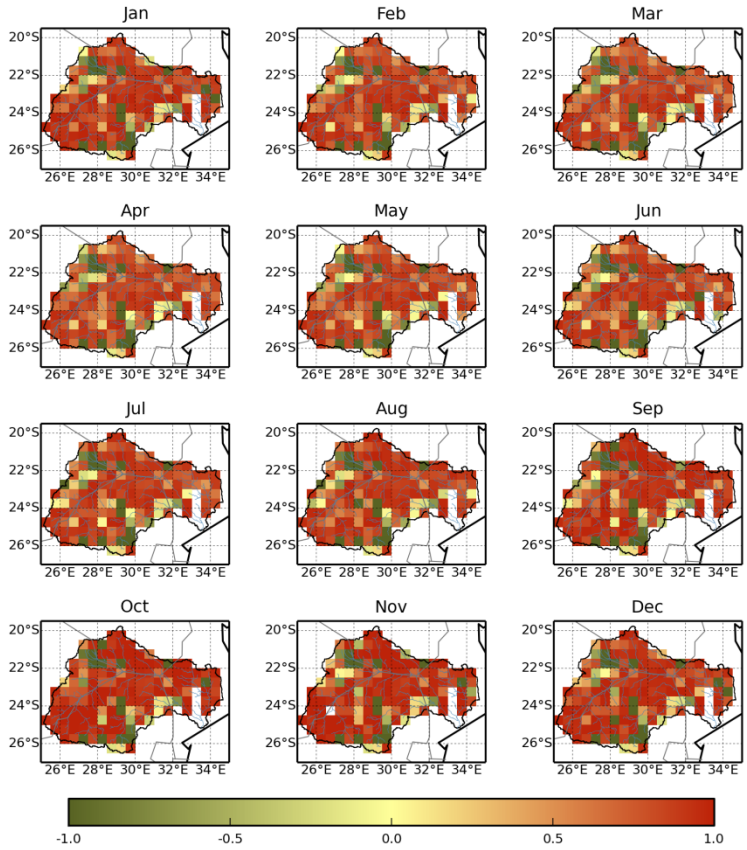

Figure 12 Mean of the monthly relative bias *RB* for subsurface flow.

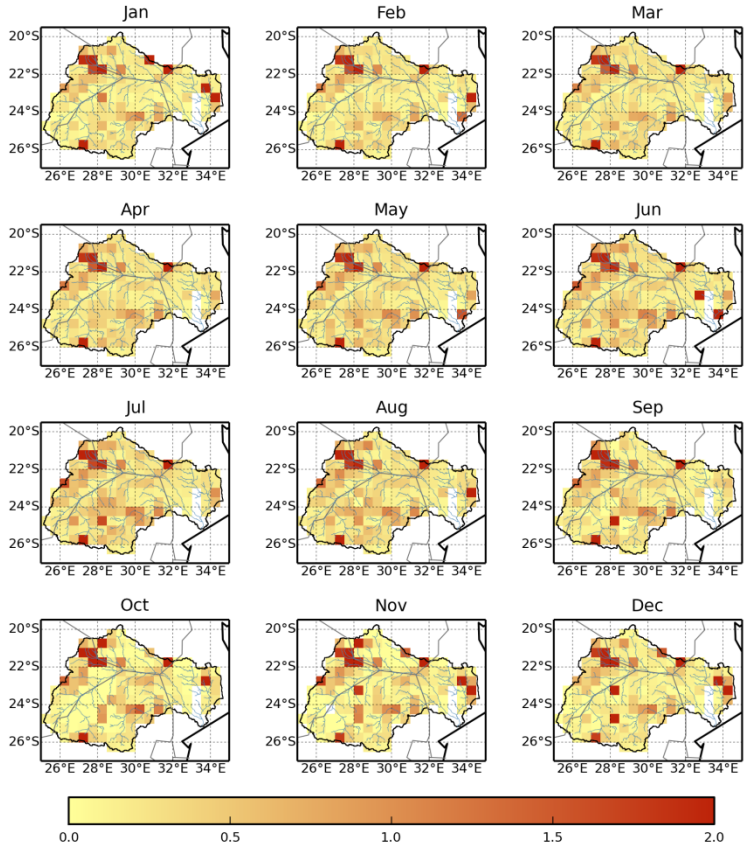

Figure 13 Standard deviation of the monthly relative bias *RB* for subsurface flow.

3.1.4 Baseflow

The mean and standard deviation from the time series of relative bias (*RB*) of the baseflow results of the two resolutions models, were computed both yearly (Figure 14) and monthly (Figure 15 and Figure 16). Baseflow is the flux with highest mean RB and standard deviations of the RB, both annually and monthly. All the green areas in the figures show that baseflow is higher for the low resolution model than for the high resolution model.

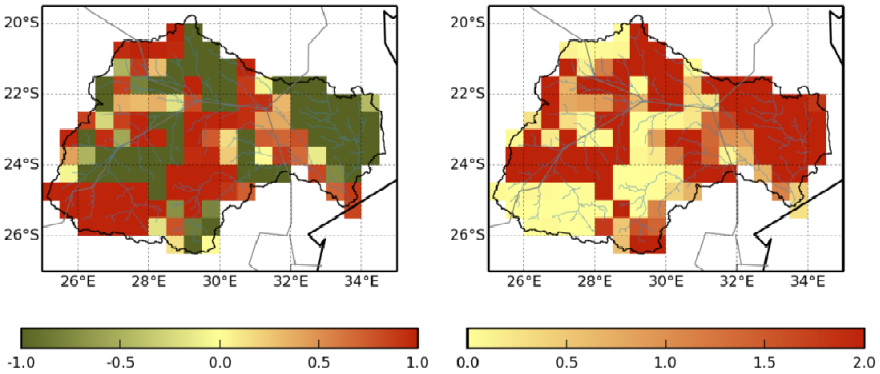

Figure 14 Mean (left) and standard deviation (right) of the annual relative bias *RB* for baseflow

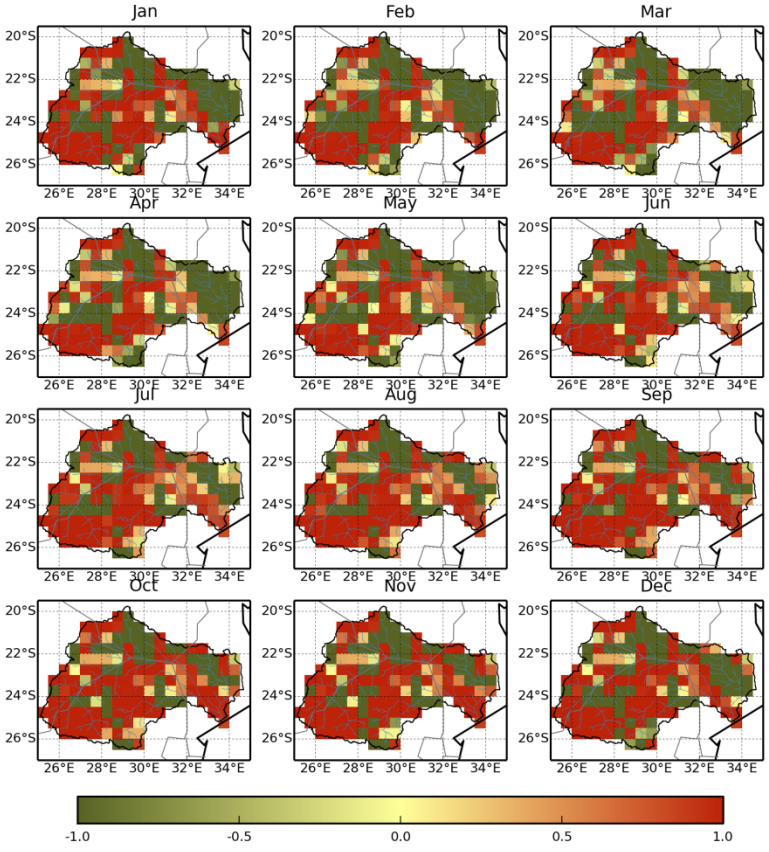

Figure 15 Mean of the monthly relative bias *RB* for baseflow

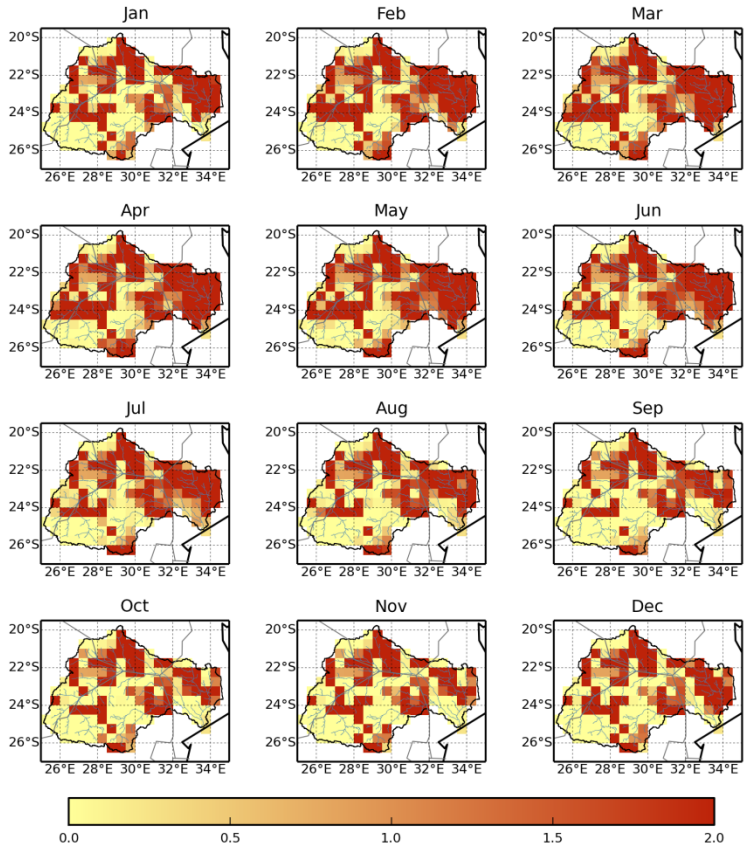

Figure 16 Standard deviation of the monthly relative bias *RB* for baseflow

3.2 VARIABILITY OF THE HIGH RESOLUTION FLUXES WITHIN EACH LOW RESOLUTION GRID CELL

The resulting time series of the coefficient of variation maps are presented in an animation. Here we summarize this result by presenting Hovmoller diagrams (time-latitude and time-longitude plots) for some longitude and latitude bands (see Figure 17).

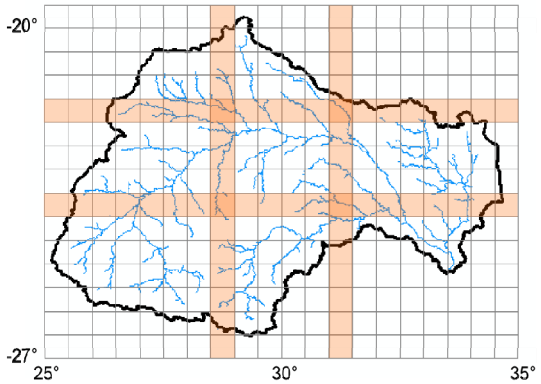

Figure 17 Chosen latitude and longitude bands for the Hovmoller diagrams.

Regarding evaporation, low coefficients of variation (CV, below 1.5) can be observed for each latitude/longitude band. The highest CV generally occur each winter (dry period). Spatially, there seems to be some indication that higher CV occur in the western part of the basin (drier part) and lower CV occur in the eastern part of the basin (wetter part).

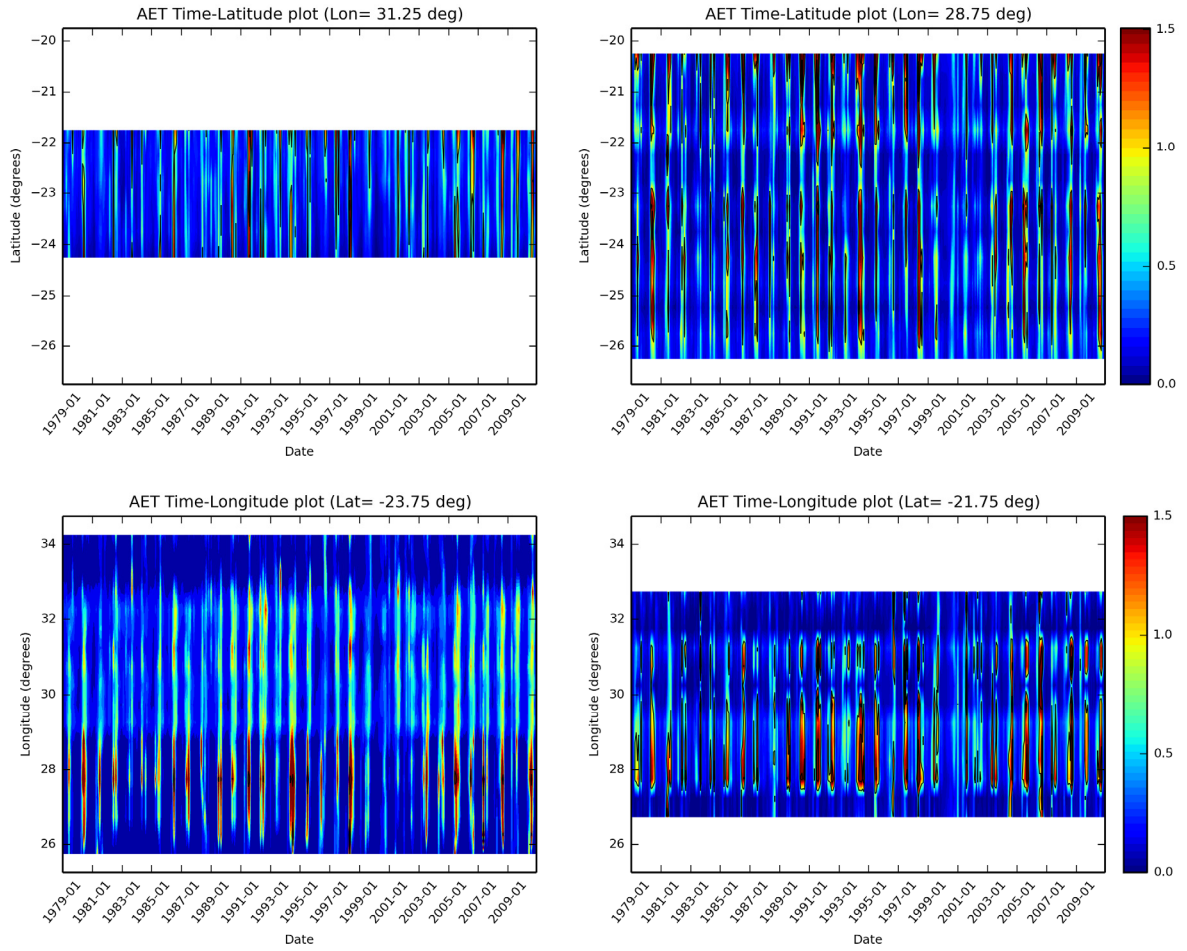

Figure 18 Latitude-time plots (top) and Longitude-time plots (bottom) of the grid (0.5°) monthly coefficient of variation of actual evaporation results from the high resolution model.

For the three runoff contributions, CV is much higher than it was for evaporation. This can be visualized from the scale. In the case of direct runoff, some horizontal bands of higher CV (red bands) can be observed in the plots, meaning that some particular cells have higher CV than others for most of the timesteps. In general, these cells are those with higher direct runoff values. Other interesting details when analysing these horizontal bands of higher CV, is that dry periods are identified by longer periods with higher CV (longer red periods) such as the drought of 1982/83 and the one of 1991/92. On the other hand, wet periods such as 1980/81, 1995/96 or the flood of 1999/2000 present low CV values which can be observed as clear interruptions of these lines.

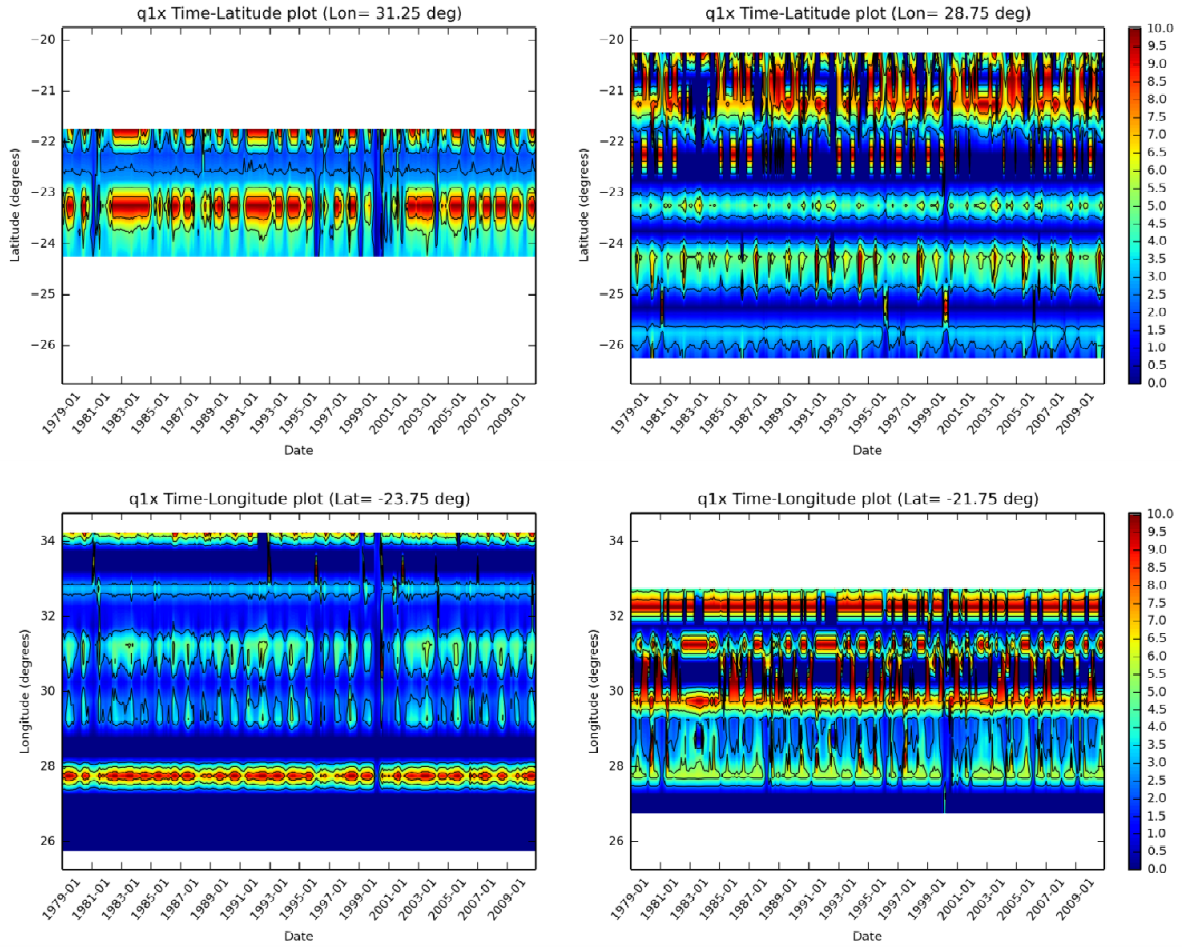

Figure 19 Latitude-time plots (top) and Longitude-time plots (bottom) of the grid (0.5°) monthly coefficient of variation of direct runoff results from the high resolution model.

Subsurface flow (Figure 20) presents similar characteristics that direct runoff, with some grid cells presenting higher CV values throughout the whole time series with short periods of low CV during wet periods.

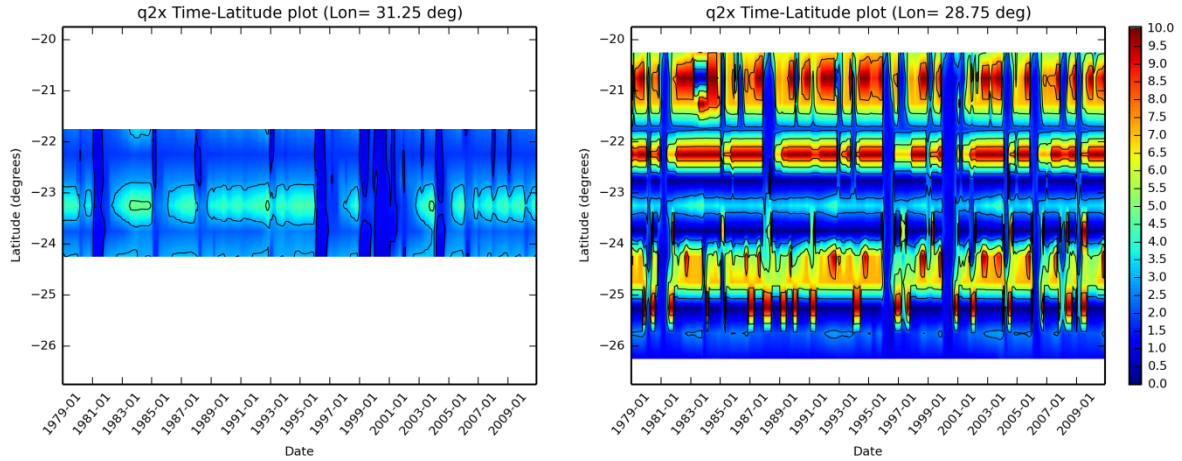

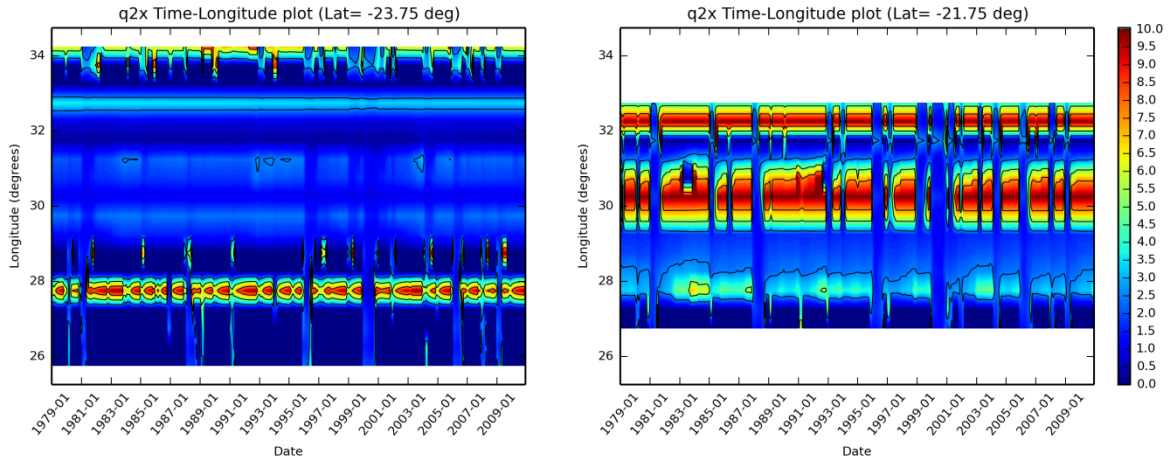

Figure 20 Latitude-time plots (top) and Longitude-time plots (bottom) of the grid (0.5°) monthly coefficient of variation of subsurface flow results from the high resolution model.

With respect to the baseflow (Figure 21) very high CV values can be observed for the entire basin until 1999. After the flood of 1999/2000 (that had a great contribution to groundwater recharge) the CV of the baseflow remained much lower for several years in some areas and for only a couple of years for other areas.

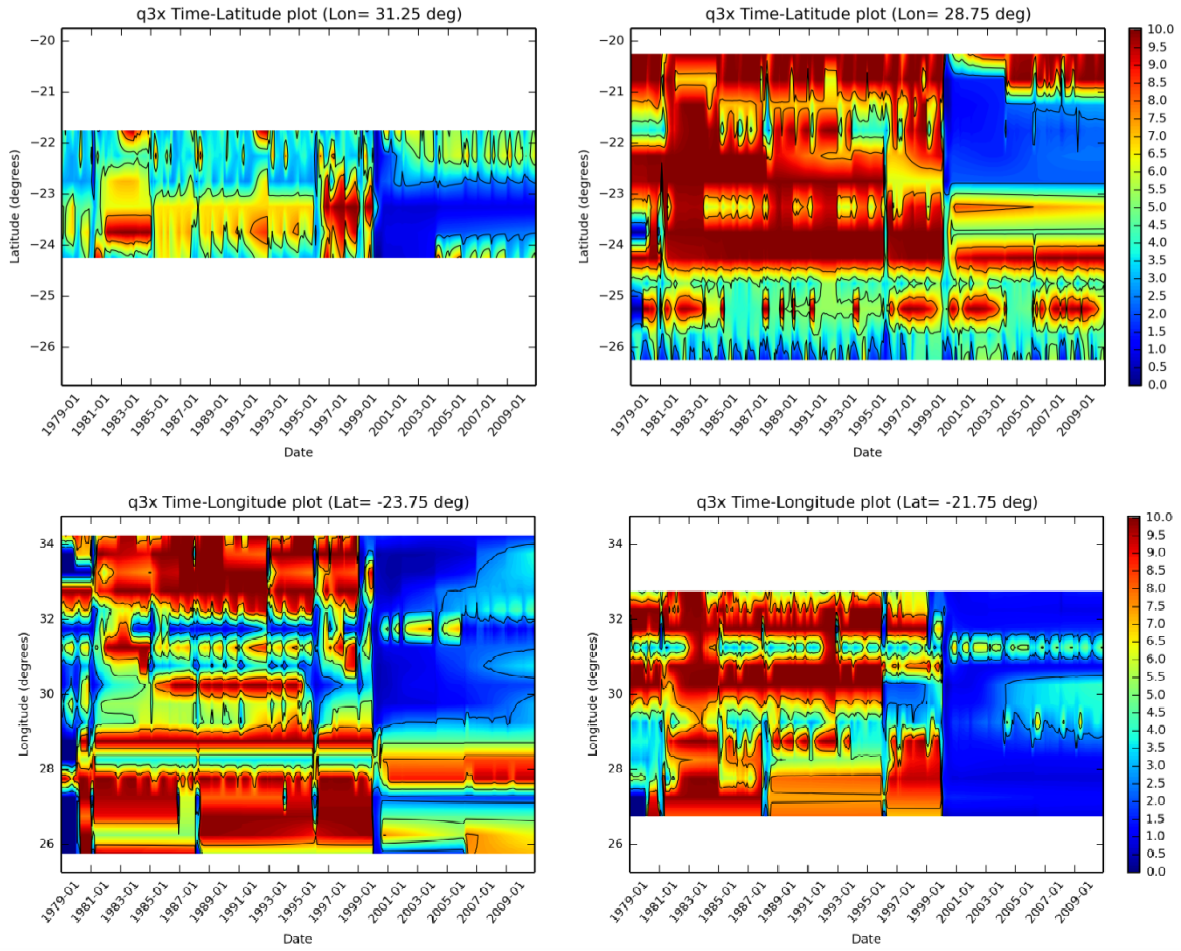

Figure 21 Latitude-time plots (top) and Longitude-time plots (bottom) of the grid (0.5°) monthly coefficient of variation of baseflow results from the high resolution model.

3.3 HYDROLOGICAL DOWNSCALING OF LOW RESOLUTION FLUXES

The HAND was computed for the Limpopo river basin for a 0.05° resolution based on the procedure described in Rennó et al. (2008) and Nobre et al. (2011). Figure 22 shows the resulting maps of HAND and slope for the Limpopo river basin. Based on the information from these two maps, wetlands area, hillslopes and plateaus were identified and mapped (Figure 23). To define these land features a number of thresholds need to be defined: 1) a contributing area threshold which defines the density of the drainage network necessary for HAND, 2) a threshold to separate HAND in land features, and 3) a threshold to separate slope in land features. These thresholds need to be compared with ground measurements and optimized. We based our threshold definition from previous studies (Rennó et al., 2008;Nobre et al., 2011) but a more comprehensive optimization will be done for this basin in a subsequent stage of this study. For this initial assessment the thresholds of 15 m and 5% are used for HAND and slope, respectively.

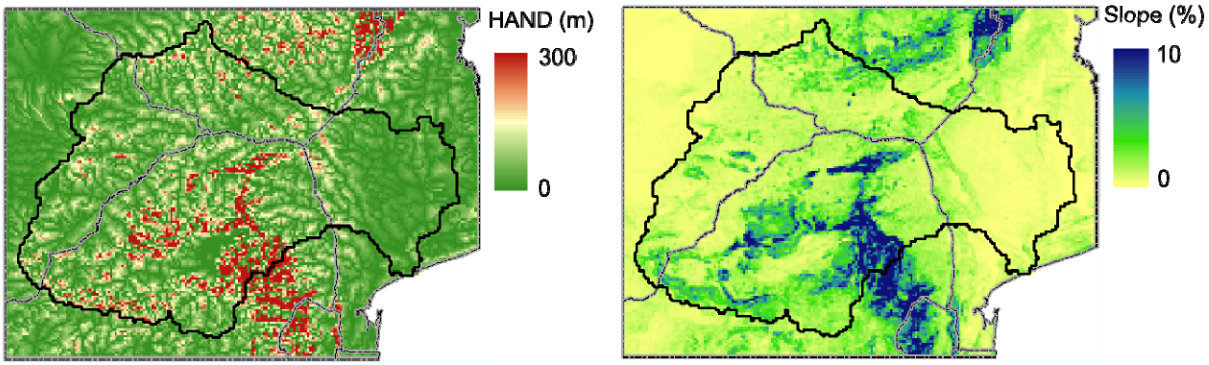

Figure 22 HAND (left) and Slope (right) for the Limpopo river basin at a 0.05° resolution

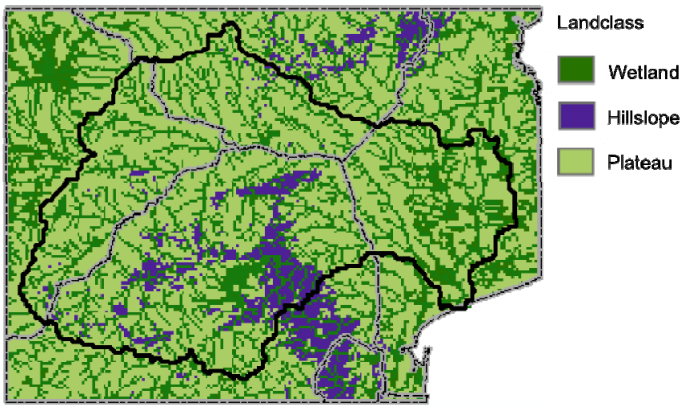

Figure 23 Land features defined based on hand and slope: HAND < 15m: wetland, HAND > 15m and S>5%: hillslope, and HAND > 15m and S < 5%: plateau.

The variability of the high resolution results within each low resolution grid cell was analyzed independently for the three land features defined. The Hovmoller diagrams of the coefficient of variation for each sub-system for selected latitudes and longitudes show that the variability of the high resolution results is to a large extent lower when distinction is made in the landscape than when no distinction is made. As an example, Figure 24 presents the time-

latitude plots for the coefficient of variation of the direct runoff for the three land features defined. When compared with Figure 19 it can be observed that the variability is lower. Another interesting feature from Figure 24 is that while wet periods are still visible as periods with low CV (blue vertical bands) for every landscape, for the plateau landscape (high hand, low slope) in the left plot (Lon=31.25°) low CV are also observed for the dry periods for some areas. This is the opposite of what was observed before and needs to be further clarified.

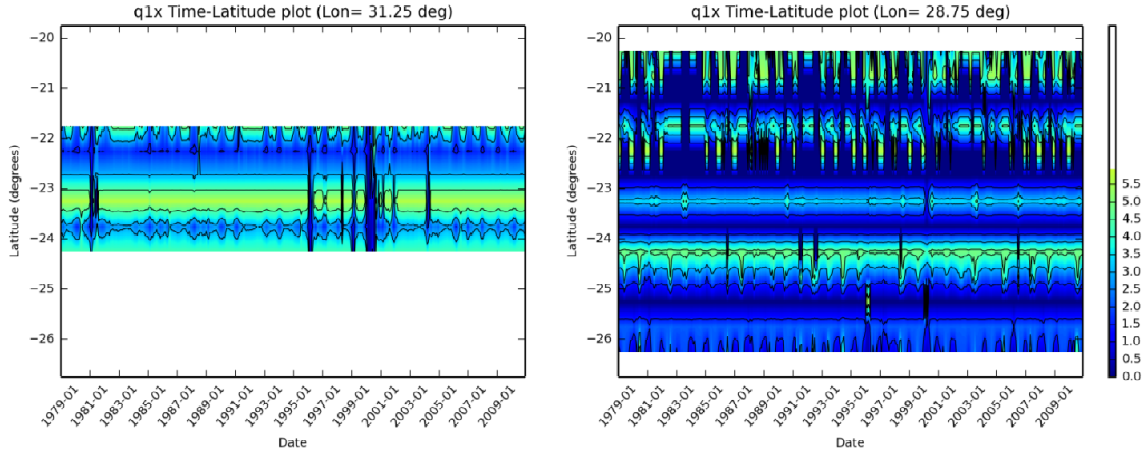

a) Wetlands

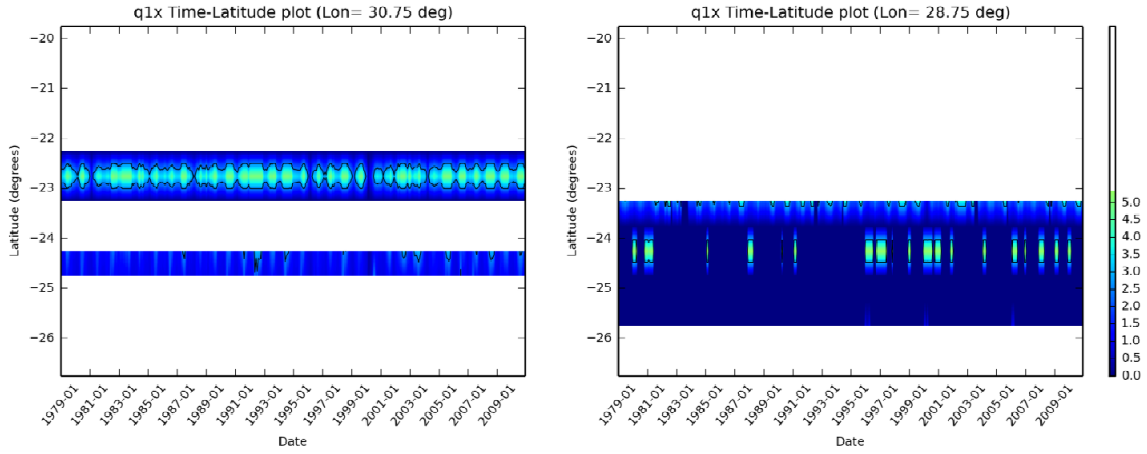

b) Hillslope

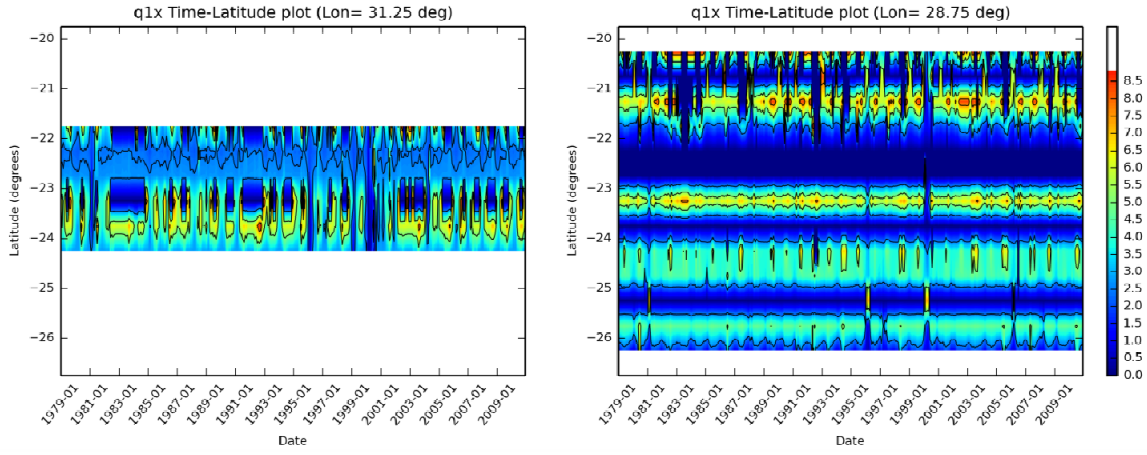

c) Plateau

Figure 24 Latitude-time plots of the grid (0.5°) monthly coefficient of variation of direct runoff results from the high resolution model for the different landscape defined.

4. CONCLUDING REMARKS

The results from two hydrological models of the Limpopo river basin both based on PCR-GLOBWB but with different spatial resolutions were compared to assess the scaling effect on the model results. For the evaporation flux the results of the two models are quite similar, and comparable results can be obtained from the low resolution model and the upscaled high resolution results. The variability of the high resolution results within each low resolution grid is also low. Evapotranspiration is mainly controlled by: (i) atmospheric demand (vapour pressure deficit), (ii) available energy, and (iii) soil moisture and vegetation conditions. In the H/L simulations the both atmospheric demand and available energy were the same (coming from ERA-Interim forcing), while only soil moisture evolution and vegetation conditions varied. Our results suggest that for evapotranspiration, the main drivers are the large scale atmospheric conditions. However, this conclusion is limited by our modelling methodology that used the same atmospheric forcing in both simulations.

The differences between resolutions in the remaining fluxes analysed were different. The results from the direct runoff analysis showed that in general this flux is zero or very close to zero in the low resolution model, and these results are consistent over time. It is quite expected to have no (or very small) direct runoff in such a low resolution model and observe an increase in this flow when resolution increases. In subsurface flow the results were more variable, meaning that the upscaled results of the low resolution model were in some areas higher and in some areas lower than the results of the high resolution model. Moreover, the time variability of these results was also higher than with direct runoff. For baseflow the results from the low resolution model are in general higher than those from the high resolution model but the time variability of these results is the highest. These results suggest that runoff, subsurface and base flow is strongly dependent on local terrain characteristics, that are enhances in the high resolution simulations, while evapotranspiration is dominated by the large-scale atmospheric conditions.

The Hovmoller diagrams, which plot the coefficient of variation of the different fluxes as a function of time, show some variability of the CV with time that allows differentiating dry and wet periods in the basin. The same diagrams but plotted individually for each land feature defined (wetland, hillslope and plateau) show that the variability of the high resolution results is to a large extent lower when distinction is made in the landscape than when no distinction is made. The analysis of the variability of the fluxes on high resolution grid cells under different land features indicates that there is good potential of downscaling the low resolution hydrological model results to high resolution based only on the terrain characteristics. The follow up of this study will explore such a possibility in more details.

5. REFERENCES

Amiotte Suchet, P., Probst, J. L., and Ludwig, W.: Worldwide distribution of continental rock lithology: Implications for the atmospheric/soil CO2 uptake by continental weathering and alkalinity river transport to the oceans, Global Biogeochemical Cycles, 17, 2003.

Balsamo, G., Boussetta, S., Lopez, P., and Ferranti, L.: Evaluation of ERA-Interim and ERA-Interim-GPCP-rescaled precipitation over the USA, ECMWF ERA Report Series 5, 1-25, available at: http://www.ecmwf.int/publications/library/do/references/list/782009, 2010.

Blöschl, G.: Statistical Upscaling and Downscaling in Hydrology, in: Encyclopedia of Hydrological Sciences, John Wiley & Sons, Ltd, 2006.

Bluth, G. J., and Kump, L. R.: Phanerozoic paleogeology, Am. J. Sci, 291, 284-308, 1991.

Dee, D. P., Uppala, S. M., Simmons, A. J., Berrisford, P., Poli, P., Kobayashi, S., Andrae, U., Balmaseda, M. A., Balsamo, G., Bauer, P., Bechtold, P., Beljaars, A. C. M., van de Berg, L., Bidlot, J., Bormann, N., Delsol, C., Dragani, R., Fuentes, M., Geer, A. J., Haimberger, L., Healy, S. B., Hersbach, H., Hólm, E. V., Isaksen, L., Kållberg, P., Köhler, M., Matricardi, M., McNally, A. P., Monge-Sanz, B. M., Morcrette, J. J., Park, B. K., Peubey, C., de Rosnay, P., Tavolato, C., Thépaut, J. N., and Vitart, F.: The ERA-Interim reanalysis: configuration and performance of the data assimilation system, Quart. J. Roy. Meteor. Soc., 137, 553-597, 10.1002/qj.828, 2011.

DEWFORA: WP4-D4.5 - Available continental scale hydrological models and their suitability for Africa, DEWFORA project - EU FP7, 2011.

DEWFORA: WP6-D6.1 - Implementation of improved methodologies in comparative case studies - Inception report for each case study, DEWFORA Project - EU FP7, www.dewfora.net, 2012a.

DEWFORA: WP4-D4.7 - Downscaled and tailor made hydrological models for the Limpopo and Niger case study basins, DEWFORA project - EU FP7 2012b.

Dürr, H. H., Meybeck, M., and Dürr, S. H.: Lithologic composition of the Earth's continental surfaces derived from a new digital map emphasizing riverine material transfer, Global Biogeochemical Cycles, 19, GB4S10, doi: 10.1029/2005GB002515, 2005.

FAO: Irrigation Potential in Africa: A Basin Approach, FAO-UN, Rome, 1997.

FAO, The digital soil map of the world (Version 3.6), FAO-UN, Rome: http://www.fao.org/geonetwork/srv/en/metadata.show?id=14116, access: August 2012, 2003.

Farmer, C. L.: Upscaling: a review, International Journal for Numerical Methods in Fluids, 40, 63-78, doi: 10.1002/fld.267, 2002.

Fowler, H. J., Blenkinsop, S., and Tebaldi, C.: Linking climate change modelling to impacts studies: recent advances in downscaling techniques for hydrological modelling, International Journal of Climatology, 27, 1547-1578, doi: 10.1002/joc.1556, 2007.

Friedl, M. A., McIver, D. K., Hodges, J. C., Zhang, X., Muchoney, D., Strahler, A. H., Woodcock, C. E., Gopal, S., Schneider, A., and Cooper, A.: Global land cover mapping from MODIS: algorithms and early results, Remote Sensing of Environment, 83, 287-302, 2002.

Fritz, S., Bartholome, E. M. C., Belward, A. S., Hartley, A., Stibig, H. J., Eva, H. D., Mayaux, P., Bartalev, S., Latifovic, R., Kolmert, S., Sarathi Roy, P., Aggarwal, S., Bingfang, W., Wenting, X., Ledwith, M., Pekel, J. f., Giri, C., Mucher, S., De Badts, E., Tateishi, R., Champeaux, J. l., and Defourny, P.: Harmonisation, Mosaicing and Production of the Global Land Cover 2000 Database, European Commission, Joint Research Center, EUR, 2003.

Hagemann, S.: An improved land surface parameter dataset for global and regional climate models, Max-Planck-Institut für Meteorologie, 2002.

Hansen, M., DeFries, R., Townshend, J. R., and Sohlberg, R.: Global land cover classification at 1 km spatial resolution using a classification tree approach, Anglais, 21, 1331-1364, 2000.

Hargreaves, G. H., and Allen, R. G.: History and Evaluation of Hargreaves Evapotranspiration Equation, Journal of Irrigation and Drainage Engineering, 129, 53-63, 2003.

Hartmann, J., and Moosdorf, N.: The new global lithological map database GLiM: A representation of rock properties at the Earth surface, Geochemistry, Geophysics, Geosystems, 13, Q12004, doi: 10.1029/2012gc004370, 2012.

Hewitson, B., and Crane, R.: Climate downscaling: techniques and application, Climate Research, 07, 85-95, 10.3354/cr0007085, 1996.

Huffman, G. J., Adler, R. F., Bolvin, D. T., and Gu, G.: Improving the global precipitation record: GPCP version 2.1, Geophys. Res. Lett, 36, L17808, doi:10.1029/2009GL040000, 2009.

LBPTC: Joint Limpopo River Basin Study Scoping Phase. Final Report. BIGCON Consortium., Limpopo Basin Permanent Technical Committee, 2010.

Loveland, T. R., Reed, B. C., Brown, J. F., Ohlen, D. O., Zhu, Z., Yang, L., and Merchant, J. W.: Development of a global land cover characteristics database and IGBP DISCover from 1 km AVHRR data, Journal of Remote Sensing, 21, 1303--1330, 2000.

Maskey, S., and Trambauer, P.: Modelling Hydrological Droughts in a (Semi-)Arid Basin, 8th Internation Conference of EWRM on Water Resources Management in an Interdisciplinary and Changing Context, Porto, Portugal, 2013,

Moriasi, D., Arnold, J., Van Liew, M., Bingner, R., Harmel, R., and Veith, T.: Model evaluation guidelines for systematic quantification of accuracy in watershed simulations, Transactions of the ASABE, 50, 885-900, 2007.

Nobre, A. D., Cuartas, L. A., Hodnett, M., Rennó, C. D., Rodrigues, G., Silveira, A., Waterloo, M., and Saleska, S.: Height Above the Nearest Drainage – a hydrologically relevant new terrain model, Journal of Hydrology, 404, 13-29, doi: http://dx.doi.org/10.1016/j.jhydrol.2011.03.051, 2011.

Peng, G.: Accuracies of Global Land Cover Maps Checked against Fluxnet Sites, Science Foundation in China, 16, 31, 2008.

Rennó, C. D., Nobre, A. D., Cuartas, L. A., Soares, J. V., Hodnett, M. G., Tomasella, J., and Waterloo, M. J.: HAND, a new terrain descriptor using SRTM-DEM: Mapping terra-firme rainforest environments in Amazonia, Remote Sensing of Environment, 112, 3469-3481, doi: http://dx.doi.org/10.1016/j.rse.2008.03.018, 2008.

Savenije, H. H. G.: HESS Opinions "Topography driven conceptual modelling (FLEX-Topo)", Hydrol. Earth Syst. Sci., 14, 2681-2692, doi: 10.5194/hess-14-2681-2010, 2010.

Shuttleworth, W. J., Yang, Z. L., and Arain, M. A.: Aggregation rules for surface parameters in global models, Hydrol. Earth Syst. Sci., 1, 217-226, doi: 10.5194/hess-1-217-1997, 1997.

Siebert, S., Döll, P., Feick, S., Hoogeveen, J., and Frenken , K.: Global Map of Irrigation Areas version 4.0.1, ed: Johann Wolfgang Goethe University, Frankfurt am Main, Germany / Food and Agriculture Organization of the United Nations, Rome, Italy, 2007.

Stewart, J. B., Engman, E. T., Feddes, R. A., and Kerr, Y.: Scaling up in hydrology using remote sensing, John Wiley and Sons, 255 pp., 1996.

Szczypta, C., Calvet, J. C., Albergel, C., Balsamo, G., Boussetta, S., Carrer, D., Lafont, S., and Meurey, C.: Verification of the new ECMWF ERA-Interim reanalysis over France, Hydrology and Earth System Sciences, 15, 647-666, 2011.

Trambauer, P., Dutra, E., Maskey, S., Werner, M., Pappenberger, F., van Beek, L. P. H., and Uhlenbrook, S.: Comparison of different evaporation estimates over the African continent, Hydrol. Earth Syst. Sci. Discuss., 10, 8421-8465, doi: 10.5194/hessd-10-8421-2013, 2013.

Trambauer, P., Maskey, S., Winsemius, H., Werner, M., and Uhlenbrook, S.: A review of continental scale hydrological models and their suitability for drought forecasting in (sub-Saharan) Africa, Physics and Chemistry of the Earth, Parts A/B/C, doi: http://dx.doi.org/10.1016/j.pce.2013.07.003, 2013

USGS EROS, Hydro1K Africa http://eros.usgs.gov/#/Find_Data/Products_and_Data_Available/gtopo30/hydro/africa, access: 2012, 2006.

van Beek, L. P. H.: Forcing PCR-GLOBWB with CRU data, Utrecht University, 2008.

van Beek, L. P. H., and Bierkens, M. F. P.: The Global Hydrological Model PCR-GLOBWB: Conceptualization, Parameterization and Verification, Utrecht University, Faculty of Earth Sciences, Department of Physical Geography, Utrecht, The Netherlands, 2009.

Wechsler, S. P.: Uncertainties associated with digital elevation models for hydrologic applications: a review, Hydrol. Earth Syst. Sci., 11, 1481-1500, doi: 10.5194/hess-11-1481-2007, 2007.

Wigmosta, M., and Prasad, R.: Upscaling and Downscaling – Dynamic Models, in: Encyclopedia of Hydrological Sciences, John Wiley & Sons, Ltd, 2006.